Investigation of multiple roots of the resistive wall mode dispersion relation, including kinetic effects

J. W. Berkery,[1] R. Betti,[2] and S. A. Sabbagh[1]
[1]*Department of Applied Physics and Applied Mathematics, Columbia University, New York, New York 10027, USA*
[2]*Princeton Plasma Physics Laboratory, Princeton University, Princeton, New Jersey 08543, USA*

(Received 13 April 2011; accepted 7 June 2011; published online 5 July 2011)

The resistive wall mode instability in tokamak plasmas has a complex frequency which can be determined by a dispersion relation that is cubic, in general, leading to three distinct roots. A simplified model of the dispersion relation, including kinetic effects, is presented and used to explore the behavior of these roots. By changing the plasma rotation frequency, it is shown that one root has a slow mode rotation frequency (less than the inverse wall time) while the other two rotate more quickly, one leading and one lagging the plasma rotation frequency. When realistic experimental parameters from the National Spherical Torus Experiment [M. Ono *et al.*, Nucl. Fusion **40**, 557 (2000)] are used, however, only one slow rotating, near-marginal stability root is found, consistent with present experiments and more detailed calculations with the MISK code [B. Hu *et al.*, Phys. Plasmas **12**, 057301 (2005)]. Electron collisionality acts to stabilize one of the rotating roots, while ion collisionality can stabilize the other. In devices with low rotation and low collisionality, these two rotating roots may manifest themselves, but they are likely to remain stable. © *2011 American Institute of Physics*. [doi:10.1063/1.3604948]

I. INTRODUCTION

The resistive wall mode (RWM) in a tokamak fusion plasma is a mode of instability related to an MHD kink-ballooning mode, but slowed considerably to grow on a time scale of the penetration of magnetic perturbations through a close-by resistive wall, τ_w (Ref. 1). Passive or active control of the RWM growth must be employed to avoid unfavorable results in tokamaks, such as disruption of the plasma current and termination of the discharge.[2]

Theoretically, the RWM non-axisymmetrically perturbs the equilibrium position of the plasma according to $\xi = \tilde{\xi} e^{-i\omega t}$. A dispersion relation can be written for the RWM that relates the mode frequency to other parameters. The complex mode frequency is written explicitly here as $\omega = \omega_r + i\gamma$, so that ω_r is the real mode rotation frequency and γ is the growth rate. When $\gamma > 0$, the mode grows exponentially. When $\gamma < 0$, the mode is said to be present but stable, as its growth is damped.

Theoretical RWM stability models leading to a cubic dispersion relation have been previously studied.[3–5] In Fitzpatrick and Aydemir's model,[4] the cubic order results from the inclusion of finite inertia, and ω_r and γ were parameterized vs. edge plasma rotation and radial wall location. It was found that one root was always stable. The other two were designated the resistive wall mode or the external kink mode based upon both the time scale of their growth rates (wall time or Alfvén time, respectively) and of their mode rotation frequencies, with the RWM always close to zero rotation and the external kink often with mode rotation close to the plasma rotation. There existed a region of wall radius where one root transitioned to the other, the RWM always remaining identified with the slowly rotating root, which could jump from stable to unstable in the transition region.

Kinetic effects were subsequently added to the stability models: first through bounce frequency resonances[6] and later by extension to the lower frequency precession drift resonance.[7] Liu *et al.* recognized that RWM stability models with kinetic effects have a dispersion relation which is still cubic in nature even without finite inertial effects.[8–10] There should therefore exist three separate possible modes of instability. These three roots are to be distinguished from the separate possibility of "multiple modes" which can also simultaneously exist with separate mode numbers (and therefore separate dispersion relations).[11] The possible resulting confluence of modes from multiple roots could be detrimental to the performance of active feedback systems that are designed to respond to only a single mode.

In the full perturbative calculation of the MISK code[12] for experimental equilibria from the National Spherical Torus Experiment (NSTX) (Ref. 13), only one root is found. A simplified model is used here in order to calculate the growth rate of the three roots and to gain tractable insight into their nature. Examination of the physical meaning of these roots, including kinetic effects, their rotation, and stability dependence on various important parameters, and whether they are actually important in more than a mathematical sense (i.e., whether they can actually be manifested in a tokamak experiment), is the purpose of the present study.

In Sec. II, an expression for the general RWM dispersion relation is presented as well as certain simplifying assumptions that lead to a more tractable model. In Sec. III, both the full MISK calculation and a simplified model with realistic parameters for NSTX are shown to lead to only one root, with near-zero natural mode rotation and near-marginal stability. The two other, more highly rotating, roots are recovered by relaxing certain parameters away from present

experimental values. The parametric dependencies of the simplified dispersion relation on plasma rotation and collisionality, and how they affect the nature of the three roots, are then explored in Sec. IV.

II. RWM DISPERSION RELATION

The dispersion relation of the RWM can be written[7] in terms of the changes to the potential energy of the plasma with no wall, δW_∞, with a resistive wall at location b, δW_b, and due to kinetic effects, δW_K, when the equilibrium is perturbed by a small displacement, ξ

$$(\gamma - i\omega_r)\tau_w = -\frac{\delta W_\infty + \delta W_K}{\delta W_b + \delta W_K} = \frac{1-C}{\hat{\gamma}_f^{-1} + C}. \quad (1)$$

Following Refs. 8 and 9, we have defined the normalized growth rate in the absence of kinetic effects, $\hat{\gamma}_f = -\delta W_\infty / \delta W_b$, and $C = (\delta W_K)/(-\delta W_\infty)$. The dispersion relation can be written in such a way that roots are found for values of (ω_r, γ) that cause $|D| = 0$, where

$$D = (\hat{\gamma} - i\hat{\omega}_r)\left(\hat{\gamma}_f^{-1} + C\right) - 1 + C, \quad (2)$$

$\hat{\omega}_r = \omega_r \tau_w$ and $\hat{\gamma} = \gamma \tau_w$.

It is through δW_K that Eq. (1) becomes non-linear, as δW_K itself depends on ω_r and γ. This kinetic term can be calculated in full using codes such as MISK, MARS-K,[8] and HAGIS.[14] Such a calculation will be performed in Sec. III with MISK for NSTX.

A. Simplified model with energy dependence

In order to make the problem tractable enough that some insight can be gained into the nature of the roots, we will see that it will become necessary to make some simplifying assumptions. We will make an effort, however, to keep the simplifications to a minimum, in order to best represent a realistic scenario. We will consider only trapped thermal particles, and will neglect the bounce frequency, thereby effectively only considering particles with $l = 0$ bounce harmonic. Energetic particles (EPs) are also important to RWM stability.[15–18] If their effects are dominant over thermal particles, they may alter the nature of the roots.[10] However for NSTX, it has been shown that EPs change RWM stability through a force that resists flux compression, so δW_K from EPs is mostly independent of plasma rotation[17] and EP collisionality.[19] In this case, the effects of EPs would be like a constant additive to C, which does not affect the characteristic nature of the roots, and will therefore be neglected in this discussion.

We now consider simplifications to the thermal particle profiles and related frequencies that will also preserve the characteristics of the roots, yet allow a tractable analysis. Let us first assume $n_i = n_e$ and $T_i = T_e$. Also, let us consider all frequencies to be constant with respect to magnetic flux coordinate or radius. Later, this will be shown to be a reasonable assumption in the region where the RWM eigenfunction is large. This assumption effectively places the radial dependence of our model on the RWM eigenfunction, rather than the fact that the plasma rotation is stronger in the core than at the edge, for example. Finally, the precession drift frequency, ω_D, will be considered independent of the pitch angle. As we will see, ω_D appears in the denominator of an expression for C along with the difference between the plasma and mode rotation frequencies. In general, ω_D is a small perturbation on this differential rotation unless the plasma and the mode are in resonance. We will also see that whether or not energy dependence is included in ω_D does change the quantitative value of the growth rate and mode rotation frequency of the roots but does not qualitatively change their nature. We expect that by neglecting the pitch angle dependence, a similar effect is obtained.

These assumptions therefore greatly simplify the calculation of δW_K, as only energy dependence is retained in the frequency resonance fraction, while not fundamentally changing the characteristic dependence of δW_K, and thus the behavior of the roots, on the various frequencies. Let us finally define some normalizations. For energy, $\hat{\varepsilon} = \varepsilon / T$, otherwise $\hat{x} = x\tau_w$, where x represents any frequency. Finally $\bar{x}$ is the constant value of $\hat{x}$ at $\hat{\varepsilon} = 1$. Then using the definition of δW_K from Ref. 17, Eq. (4), we can write

$$C = c\frac{8}{15\sqrt{\pi}}\int_0^\infty \left[\left(\frac{\hat{\omega}_{*N} + \left(\hat{\varepsilon} - \frac{3}{2}\right)\hat{\omega}_{*T} + \hat{\omega}_E - \hat{\omega}_r - i\hat{\gamma}}{\overline{\omega_D}\hat{\varepsilon}^{a_1} - i\bar{\nu}\hat{\varepsilon}^{a_2} + \hat{\omega}_E - \hat{\omega}_r - i\hat{\gamma}}\right)_i + \left(\frac{-\hat{\omega}_{*N} - \left(\hat{\varepsilon} - \frac{3}{2}\right)\hat{\omega}_{*T} + \hat{\omega}_E - \hat{\omega}_r - i\hat{\gamma}}{-\overline{\omega_D}\hat{\varepsilon}^{a_1} - i\sqrt{2m_i/m_e}\bar{\nu}\hat{\varepsilon}^{a_2} + \hat{\omega}_E - \hat{\omega}_r - i\hat{\gamma}}\right)_e\right]\hat{\varepsilon}^{\frac{5}{2}}e^{-\hat{\varepsilon}}d\hat{\varepsilon}. \quad (3)$$

The first term in the integral is for trapped ions, while the second is for trapped electrons. The ω_{*N} and ω_{*T} terms are the density and temperature components of the diamagnetic frequency ($\omega_* = \omega_{*N} + \omega_{*T}$), which have opposite sign for ions and electrons. The $E \times B$ frequency is defined as $\omega_E = \omega_\phi - \omega_*$, which results from radial force balance, neglecting poloidal rotation.[12,20] Here ω_ϕ is the plasma toroidal rotation.

In the denominator, ω_D is the precession drift frequency, which also changes sign between ions and electrons. We have written the equation with $\overline{\omega_D}$ to make the energy dependence of this term explicit. Normally, a_1 should be equal to one, but we can set it equal to zero to remove the energy dependence of the precession drift frequency for analysis purposes. Similarly, $\bar{\nu}$ is the ion collisionality at thermal energy, and we can use $a_2 = 0$ or $-\frac{3}{2}$. Note that for deuterium ions, $\sqrt{2m_i/m_e} \approx 86$, so electron collisionality is generally much larger.[19]

Finally, here c is a constant which represents the completed integration over pitch angle, χ, and magnetic surface, Ψ, of all the other terms in the full δW_K calculation not inside the energy integral

$$c = \frac{15\sqrt{\pi}}{(-\delta W_\infty)8}\sum_j \int\int |\langle H/\hat{\varepsilon}\rangle|^2 n_j T_j \frac{\hat{\tau}}{B}|\chi| d\chi d\Psi, \quad (4)$$

where $H/\hat{\varepsilon}$ and $\hat{\tau}$ are defined in Ref. 21. Note that the mode eigenfunction, $\xi_\perp$ appears in H only. No assumptions about $\xi_\perp$

have been made except that it is unchanged by kinetic effects.[17] The constant c is roughly proportional to $\beta/(-\delta W_\infty)$, where β is a measure of the ratio of plasma pressure to magnetic pressure.

Technically, our assumptions of $\omega_{*N}(\Psi)$, $\omega_{*T}(\Psi)$, and $\bar{\nu}(\Psi)$ all being constant are inconsistent, as $\omega_{*n} \propto (T/n)(dn/d\Psi)$ and $\omega_{*T} \propto dT/d\Psi$ imply $n \propto T \propto \Psi$, while $\bar{\nu} \propto nT^{-\frac{3}{2}}$. Nevertheless, we will treat them each as constants for simplicity.

B. Further simplified model without energy dependence

Liu *et al.* presented a simplified, analytical form of Eq. (3), in which there are no energy dependencies in the frequency resonance fractions.[9] It can be recovered under the following assumptions: $\omega_{*T}=0$, $a_1=0$, and $a_2=0$. Then the energy integral can be easily performed, resulting in a constant, and we find

$$C = c\left[\frac{\hat{\omega}_{*N}+\hat{\omega}_E-\hat{\omega}_r-i\hat{\gamma}}{\hat{\omega}_D-i\hat{\nu}+\hat{\omega}_E-\hat{\omega}_r-i\hat{\gamma}} + \frac{-\hat{\omega}_{*N}+\hat{\omega}_E-\hat{\omega}_r-i\hat{\gamma}}{-\hat{\omega}_D-i\sqrt{2m_i/m_e}\hat{\nu}+\hat{\omega}_E-\hat{\omega}_r-i\hat{\gamma}}\right]. \quad (5)$$

Additionally in Ref. 9, only the $\hat{\nu}=0$ collisionless case was considered. An analytical solution for this collisionless case is discussed in Appendix B.

III. EXPERIMENTAL CALCULATION OF GROWTH RATE AND MODE ROTATION FREQUENCY

The MISK code is used to calculate the stability of high β plasmas in NSTX.[17,22,23] The full MISK calculation for NSTX discharge 133456 at 0.577 s, using experimentally measured input profiles of various frequencies (shown in Fig. 1), results in a single root, with $\hat{\omega}_r=0.012$ and $\hat{\gamma}=-0.2$. The fluid growth rate was calculated to be $\hat{\gamma}_f=0.62$ for this equilibrium, from $\delta W_\infty = -1.97\times10^{-2}$ and $\delta W_b = 3.17\times10^{-2}$.

The ω_E profile shown in Fig. 1, measured with charge exchange recombination spectroscopy, is from just before the RWM experimentally goes unstable the experimental detection of an unstable RWM. Often during experiments, the plasma rotation decreases with time during the discharge, whether naturally or due to applied non-resonant magnetic braking.[24] When the ω_ϕ profile is scaled in this calculation from three times down to one times the experimentally marginally stable profile, the trajectory in $(\hat{\omega}_r,\hat{\gamma})$ space is indicated by the dashed line in Fig. 2. A crossing of this line into positive $\hat{\gamma}$ would indicate that the calculation predicts instability, consistent with the experimental result. We can see that the result comes quite close (within $\hat{\gamma}\sim0.05$) in its prediction.[17]

Only one root is found with the full MISK calculation, even when $\hat{\omega}_r$ and $\hat{\gamma}$ from the left hand side of Eq. (1) are iterated back into the right hand side. The iterative root-finding method for the perturbative approach is not practical for finding multiple roots, as it does not consistently converge on all of the solutions. This phenomenon is discussed in detail in Appendix A.

We will now use our simplified model of Sec. II to gain further insight and to try to find more than one solution. The roots of the RWM dispersion relation are found by setting $D=0$ in Eq. (2). Using the analytical approximation of Eq. (5), this can be done relatively straightforwardly using MATHEMATICA. When the energy integral of Eq. (3) is included, finding the roots requires more effort. Here, we use a FORTRAN code which performs the energy integration that is at the core of the MISK code. MISK is a perturbative code, in the sense that values of $(\hat{\omega}_r,\hat{\gamma})$ are not found self consistently, but rather must be input into Eq. (3) to find C. Therefore, we use a brute-force trial and error approach, where a grid of values of $(\hat{\omega}_r,\hat{\gamma})$ (generally from -10 to 10) are input into Eq. (3) to determine C and then Eq. (2) to determine D, and a plot of contours of $1/|D|$ vs. $(\hat{\omega}_r,\hat{\gamma})$ is produced which shows the values of $(\hat{\omega}_r,\hat{\gamma})$ where $D\rightarrow0$. Such a plot is shown in Fig. 2 (with magnified axes).

The assumptions made to simplify the expression for δW_K limit our ability to make a detailed comparison with experiments. The fact that the profiles in Fig. 1 are not constant demonstrates the extent of the model simplifications. However, we will attempt to make the calculation as realistic as possible within those constraints. We will use the full

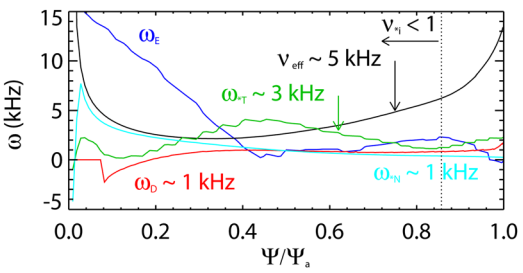

FIG. 1. (Color online) Profiles of various frequencies vs. normalized poloidal magnetic flux for NSTX discharge 133456 at 0.577 s. Approximate average values are indicated. The precession drift and collision frequencies are at thermal energy, and ω_D is also taken at zero pitch angle. The vertical dashed line indicates the location where ν_{*i}, the ratio of the effective collision frequency to the bounce frequency, is one.

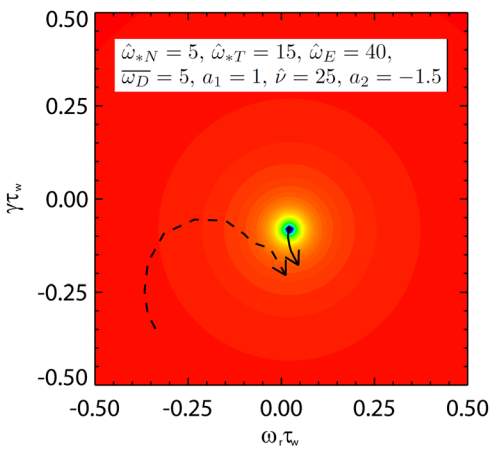

FIG. 2. (Color online) Contours of $1/|D|$, showing the location of the single root in the $(\hat{\omega}_r,\hat{\gamma})$ space for the "realistic" case, and its trajectory with *decreasing* $\hat{\omega}_E$, from 40 to 0. Also shown with a dashed line is the trajectory from the full MISK calculation for NSTX discharge 133 456 at 0.577 s, also with decreasing rotation (scaled experimental ω_ϕ profile).

proper energy dependence from Eq. (3), setting $a_1 = 1$, $a_2 = -1.5$. Using the constant values indicated in Fig. 1, and a realistic $\tau_w = 5$ ms, we find that representative values are $\hat{\omega}_{*N} = 5$, $\bar{\omega}_D = 5$, $\bar{\nu} = 25$, and $\hat{\omega}_{*T} = 15$. The $E \times B$ frequency is roughly $\hat{\omega}_E \approx 0 - 10$ over the outer 60% of flux surfaces. Therefore, levels of $\hat{\omega}_E = 40 \rightarrow 0$ will be used to approximate an experimental slowing down trajectory. Finally, the value $c = 1$ will be used, so that $|C| = -|\delta W_K|/\delta W_\infty$ is in the middle of the usual range (0.5–2.5) that the full MISK calculation finds (i.e., kinetic effects are comparable to fluid effects). Figure 2 shows that with these parameters, a single root is found with near zero rotation and near marginal growth rate. Although the axes are magnified in this plot, the other two roots were not found for $\hat{\omega}_r$, $\hat{\gamma}$ between -10 and 10 ($<|2|$ kHz). The singularity shown is for $\hat{\omega}_E = 40$, and the trajectory is shown with a solid line from there down to 0. The root changes very little in $(\hat{\omega}_r, \hat{\gamma})$ space with this rotation change.

Our simplified model with "realistic" values finds $(\hat{\omega}_r, \hat{\gamma})$ similar to the full MISK calculation. The fact that the full MISK calculation trajectory changes $(\hat{\omega}_r, \hat{\gamma})$ more may be due to any number of differences in the calculations, most prominently the assumption of flat radial profiles in the model. Even with the simplified model, with realistic frequencies, we still only find one root. This is not to say that the other roots do not exist, but rather that they are outside of the domain of credible RWM frequencies in our analysis by being either highly rotating and/or highly stabilized or destabilized. One candidate for this behavior is a collisional plasma, which one might imagine could require a large negative $\hat{\gamma}$ in the denominator of Eq. (3) to balance the imaginary terms for a solution to exist. In Sec. IV, we will consider the parametric dependence of the roots on various quantities individually to gain further insight.

IV. PARAMETRIC DEPENDENCE OF THE DISPERSION RELATION

There are several important parameters for RWM stability that have been explored in experiments, as well as comparisons between experiments and theory, including plasma rotation and collisionality. Here, we will consider simplified cases to attempt finding more than one root and to explore the dependencies of the multiple roots on these same parameters. These simplifications will necessarily reduce the realistic matching with present experiments, instead moving in the direction of future devices. For example, in Subsection IV A, we will consider the plasma to be collisionless. Additionally, we will take $\omega_{*T} = 0$, consistent with a flat temperature profile, so that the only energy dependencies in Eq. (3) are in the precession drift and collsionality terms. We will explore the effect of these energy dependencies individually in Subsections IV A and IV B as well.

A. Plasma rotation

Toroidal plasma rotation is an important variable in RWM stability.[22,25] As is often done,[8,9] we will utilize ω_E as a proxy for plasma rotation in the present analysis. Unless otherwise indicated, the values of $\hat{\gamma}_f = 2$ and $c = 0.6$ will be used in all cases presented here, to be consistent with Ref. 9. To more clearly see the effect of ω_E, in this subsection, we will consider the collisionless ($\hat{\nu} = 0$) case. Finite collisionality will be added in Subsection IV B. To avoid singularities in the energy integral of Eq. (3), the imaginary term in the denominator must be less than zero.[19] With collisions, this is normally not an issue, but when $\hat{\nu} = 0$, one can replace the limits of integration $(0, \infty)$ with two integrals, from $(0, -10i)$ and $(-10i, -10i + \infty)$ for ions, and $(0, 10i)$ and $(10i, 10i + \infty)$ for electrons.

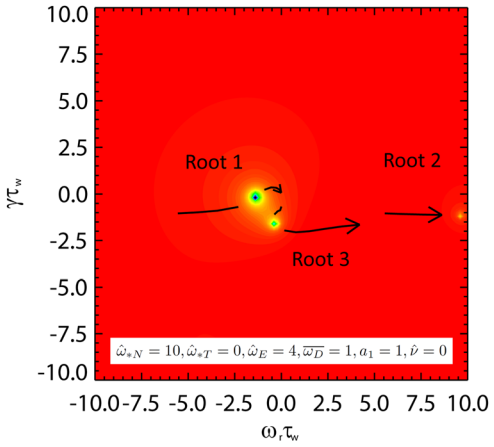

FIG. 3. (Color online) Contours of $1/|D|$, showing the location of roots in the $(\hat{\omega}_r, \hat{\gamma})$ space and their trajectories with *increasing* $\hat{\omega}_E$.

Figure 3 shows that indeed all three roots are found in the collisionless case. Here, the calculation is shown with energy-dependent $\hat{\omega}_D$ for $\hat{\omega}_E = 4$ (and trajectories over the range $0 \leq \hat{\omega}_E \leq 10$) as contours of $1/|D|$ in the manner of Fig. 2. The values for the other parameters are indicated on the plot. Note that root 2 was not followed outside of the domain shown.

Figure 4 shows the normalized growth rate and mode rotation frequencies vs. normalized $E \times B$ frequency of the three RWM roots for the same set of parameters from Fig. 3 (in red/solid lines). Also shown with blue/dashed lines on the figure are the three roots with the same parameters but with energy-independent precession drift frequency. When this collisionless analytical case is considered, the results duplicate those previously found by Liu *et al.* in Ref. 9, except for a flipped sign of $\hat{\omega}_r$ (due to a different directional definition).

The fundamental character of the roots remains the same when the change is made from energy-dependence ($a_1 = 1$) to energy-independence ($a_1 = 0$), but the patterns are generally shifted to lower $\hat{\omega}_E$, higher growth rate, and mode rotation closer to the plasma rotation.

When $\hat{\omega}_E$ becomes large, the mode rotation frequency goes to zero for one root and becomes large for the other two. When $\hat{\omega}_E$ goes to zero, one root is represented by $(0, \hat{\gamma}_3)$, while the other two are $(\pm\hat{\omega}_{r1}, \hat{\gamma}_1)$. That is, one root has no mode rotation, while the others have equal and opposite mode rotation with the same growth rate. The mathematical reason for this behavior is discussed in Appendix B.

Generally, a pattern that can be observed is that one root has a slow mode rotation ($\hat{\omega}_r \lesssim 1$) while the other two have

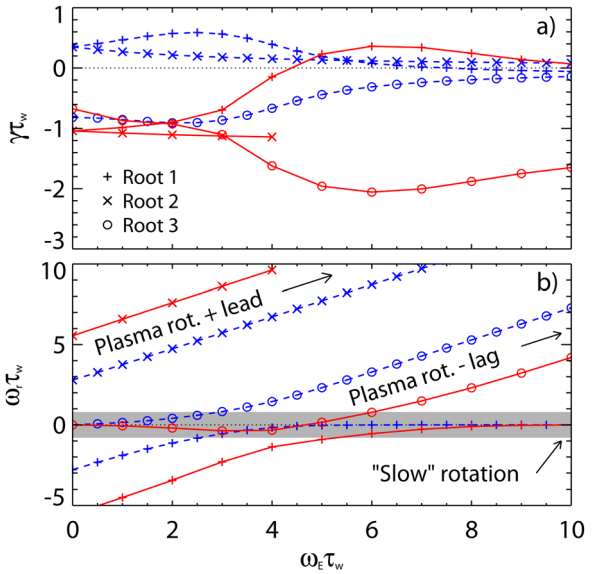

FIG. 4. (Color online) (a) Growth rate and (b) mode rotation frequency of the roots of the RWM dispersion relation, vs. $\hat{\omega}_E$. Shown in blue/dashed lines are the results from the collisionless analytical simplification of Eq. (5) ($\omega_{*T}=0$, $\hat{\nu}=0$, $a_1=0$), with parameters: $\hat{\omega}_{*N}=10$, $\hat{\omega}_D=1$, which are the same results as in Ref. 9 (with flipped sign on $\hat{\omega}_r$). In red/solid lines are the results with the same parameters, but with $a_1=1$ and $\overline{\omega_D}=1$ (energy dependent precession drift frequency). The grey region indicates slow mode rotation with respect to the wall time ($|\hat{\omega}_r| \lesssim_x 1$).

mode rotation defined by $\hat{\omega}_r = \pm\hat{\omega}_0 + \hat{\omega}_E$, where $\hat{\omega}_0$ is found in Appendix B. In other words, the modes represented by these roots rotate with the plasma, one leading and one lagging. Note that while the analytic case presents the possibility of a highly rotating unstable root (root 2), the more realistic scenario of energy-dependent ω_D does not (root 2 is stable). We can note some similarities in behavior of the roots between the present kinetic model and the Fitzpatrick and Aydemir model[4] described in the introduction. We do not find that one of the more highly rotating roots is robustly stable (although this will become possible when collisionality is added in Subsection IV B), but we do find that they have $\omega_r \sim \omega_E$, as in the previous model.

We will now define the root with near-zero mode rotation as the slow, or "*S*" root. The root leading the plasma rotation will be designated the "$R+$" root and the one lagging the "$R-$" root. We must keep in mind that one mathematical solution can transit from being the $R-$ to S root (as in root 1 in Fig. 4) or vice versa (as in root 3) as parameters are changed. This is a physically based categorization of the roots. An alternative is to track the roots as the kinetic effects are reduced to zero ($c \to 0$ in Eq. (3)) and label the particular solution that becomes the fluid solution $\left[(\hat{\omega}_r, \hat{\gamma}) \to (0, \hat{\gamma}_f)\right]$ as the RWM root. Our categorization is perhaps less clear mathematically, as one solution can transit from S to R labels, but we believe it is preferable as a physical interpretation as it always identifies the S root, which is most likely to be seen experimentally.

There is some range of $\hat{\omega}_E$ where a switchover occurs between two of the solutions, as to which one obeys which of these behaviors (slow or rotating). A similar behavior was noticed with respect to the proximity of the wall, rather than plasma rotation, in the previous model.[4] Figures 5(a) and 5(b) show a duplication of Figs. 4(a) and 4(b) for only the analytical roots 1 and 3, zoomed in on the switchover region to better see the behavior of the roots in this rotation range. Although only the analytic roots are shown here, the behavior or the energy-dependent case is quite similar. In Fig. 4, the switchover occurs between roots 1 and 3 in the range of $2 \lesssim \hat{\omega}_E \lesssim 4$, for the analytic case and $5 \lesssim \hat{\omega}_E \lesssim 7$ for the energy-dependent $\hat{\omega}_D$ case. Also shown in Figs. 5(c) and 5(d) are the real and imaginary kinetic terms, $Re(C)$ and $Im(C)$ for these roots. The switchover range is intriguing, primarily because it means that two slowly rotating modes could simultaneously exist. However, Fig. 5(a) shows that in this range one of the two is highly damped. The S root, which has $\omega_r \approx 0$, has a resonance between $\omega_D = 1$ and $\omega_E = 1$ for electrons. This makes the denominator of Eq. (5) small, so both $Re(C)$ and $Im(C)$ are large and the plasma is very stable. The S root then jumps to the other solution (root 1) at $\omega_E \approx 2.5$, which is unstable. This jump in $\hat{\gamma}$ was also analogously seen in the Fitzpatrick and Aydemir model without kinetic effects.[4] It only begins to approach marginal stability again at larger plasma rotation ($\omega_E \gtrsim 6$) as the real kinetic effects are steadily rising.

Let us now consider further what these results imply physically. For example, consider the energy-dependent case

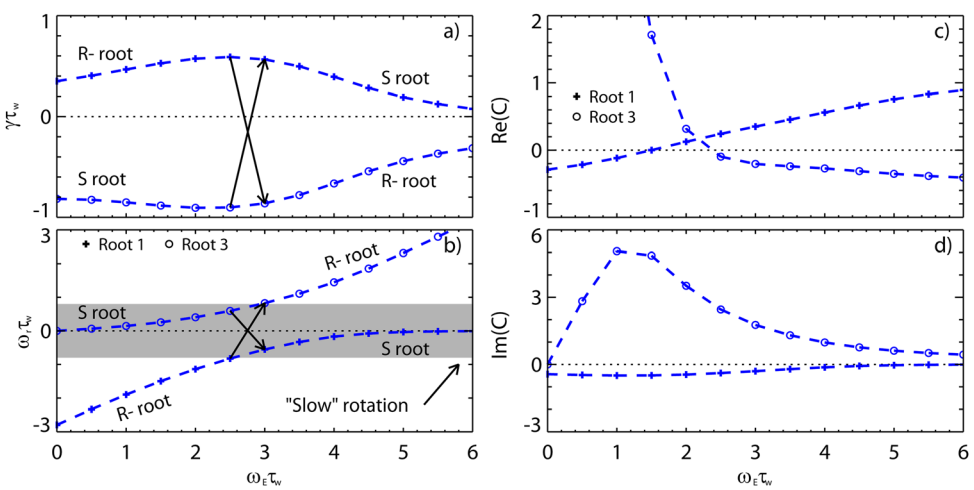

FIG. 5. (Color online) (a) Growth rate, (b) mode rotation frequency, (c) $Re(C)$, and (d) $Im(C)$ for the analytical roots 1 and 3 from Fig. 4, vs. $\hat{\omega}_E$.

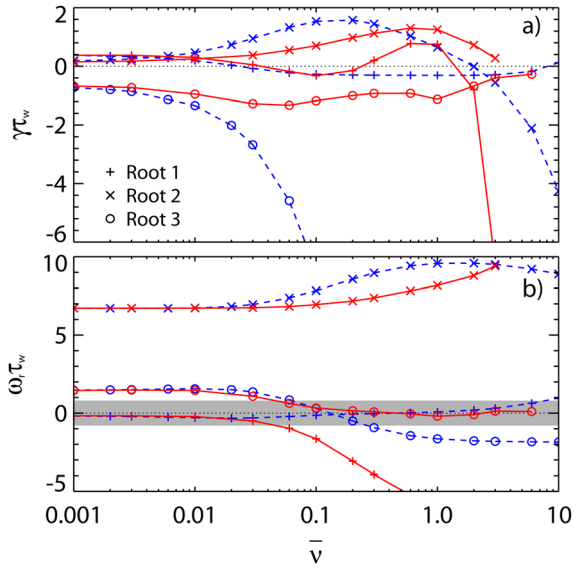

FIG. 6. (Color online) (a) Growth rate and (b) mode rotation frequency of the roots of the RWM dispersion relation, vs. $\bar{\nu}$. Shown in blue/dashed lines are the results from the analytical simplification of Eq. (5) ($\omega_{*T}=0$, $a_1=0$, $a_2=0$), with parameters: $\hat{\omega}_{*N}=10$, $\hat{\omega}_D=1$, and $\hat{\omega}_E=4$. Shown in red/solid lines are the results with the same parameters, but $a_2=-1.5$, for energy dependent collisionality.

at $\hat{\omega}_E=10$. The S root is marginally unstable, while the two R roots are stable ($\hat{\gamma}<0$) with $\hat{\omega}_r\approx 4$ and $\gg 10$. That is to say if $\tau_w=5$ ms, the plasma is rotating at 2 kHz, while there are possible damped, stable modes rotating at 800 Hz and $\gg 2$ kHz. Clearly the S root is the familiar resistive wall mode, as is seen experimentally in NSTX and other devices.

B. Collisionality

Collisionality has been shown to be an important factor in RWM stability,[19] but not in a simple way, such as being universally stabilizing.[26,27] In Ref. 19, three collisionality models were considered: collisionless, energy-independent, and energy-dependent. In Subsection IV A, we considered the collisionless case ($\hat{\nu}=0$). Here, we will consider the energy-independent case ($a_2=0$), which once again provides a convenient analytical solution (Eq. (5)) and the energy-dependent case $\left(a_2=-\frac{3}{2}\right)$. For simplicity $\hat{\omega}_D$ is considered a constant in both cases ($a_1=0$), so that we can see the effect of the energy dependence in the collisionality term alone. Because the $\sqrt{2m_i/m_e}$ term makes collisionality considerably larger for electrons, we expect that even a small $\hat{\nu}$, compared to the other frequencies, will affect the nature of the RWM roots.

Figure 6 shows $\hat{\gamma}$ and $\hat{\omega}_r$ vs. $\bar{\nu}$ with the same parameters as Fig. 4 at $\hat{\omega}_E=4$. For the analytical energy-independent collisionality case, shown in blue/dashed lines, as soon as $\hat{\nu}$ is increased to 0.01, the electron collisionality term $\sqrt{2m_i/m_e}\hat{\nu}$ becomes of order unity and begins to have a large effect on the growth rate of the $R-$root (root 3). By $\hat{\nu}=0.1$, this root is made extremely stable. The mode rotation frequency is relatively less affected by collisionality, but we do note that the $R-$root can begin to rotate in the direction opposite to the plasma when it becomes highly stabilized by electron collisions. A similar pattern does not take hold for the $R+$root (root 2) until the ion collisionality becomes of order unity itself, $\hat{\nu}\approx 1$. This description can be confirmed by examining Eq. (5) with the electron term set to zero. In that case, root 3 does not exist, and the resulting roots 1 and 2 are the same as in Fig. 6 when $\hat{\nu}\lesssim 1$.

When energy dependence is added to the collisionality term ($a_2=-1.5$), the results are the red/solid lines in Fig. 6. In general, it takes larger $\bar{\nu}$ in the energy-dependent case to have an effect on the growth rate of the roots, which is expected since the $\hat{\varepsilon}^{-\frac{3}{2}}$ greatly reduces the importance of high energy particle collisions.[19] Still, the $R-$root is highly damped above $\bar{\nu}\approx 2.5$, an order of magnitude less than that realistic NSTX value of $\bar{\nu}\approx 25$.

Finally, we note that it is the S root (root 1 in the energy-independent case and root 1 transitioning to 3 in the energy-dependent case) that remains close to marginal $\hat{\gamma}$, while the R roots are the ones stabilized by collisionality. Once again the switchover region ($\bar{\nu}\sim 0.06$) is intriguing as two roots are slowly rotating and here are weakly damped (also the $R+$root is highly rotating and unstable). Recall, however, that ω_D energy dependence, which tended to be stabilizing, was not included in this subsection.

The stabilization of one of the R roots by electron collisionality and of another by ion collisionality can be explained by examination of Eqs. (1) and (3). In order for a solution to exist with large $\hat{\omega}_r$ on the left-hand side of Eq. (1), a large $-i\hat{\nu}$ term in the denominator of Eq. (3) must be balanced with a large negative $\hat{\gamma}$. If they are not and $\hat{\gamma}$ is near marginal, then the large collisionality in the denominator causes the $\hat{\omega}_r$ on the left hand side of Eq. (1) to be close to zero. In NSTX $\bar{\nu}$ is indeed on the same order as the other frequencies (see Fig. 1), which can help explain why in Sec. III only the S root was found with realistic experimental parameters.

The physical interpretation of this result is that machines with collisionality on the order of the other important frequencies will have the rotating roots robustly stabilized, but for future devices with low rotation and an order of magnitude lower collisionality, these roots may become more important. This is in contrast to the simpler model[4] in which one of the three roots was always considered robustly stable. However, we note that even in the low rotation, low collisionality case, we do not find multiple roots with unstable or even near marginally unstable growth rates. Although the simplest collisionless cases with energy-independent ω_D could be interpreted that way (blue/dashed lines in the left side of Fig. 4(a) or either result on the left side of Fig. 6), the energy-dependence of the precession drift frequency is stabilizing, leaving only the true RWM root near marginal stability.

V. CONCLUSION

The resistive wall mode dispersion relation, including kinetic effects, is cubic and therefore allows the possibility of three distinct modes, in general. Two simplified models of the dispersion relation, analytical and energy-dependent, give qualitatively similar understanding of the behavior of these roots with respect to plasma parameters. As plasma rotation is changed, the S root maintains slow mode rotation,

while the two R roots rotate with the plasma, one leading and one lagging. It is this near-zero rotating S root that is the RWM identified in the full MISK code calculations. When collisions are included in the calculation, they can have a strongly stabilizing effect on the two R roots, first through electron collisionality which is higher, and then through ion collisionality. Using an energy-dependent collisionality model requires larger collisionality to have the same stabilizing effect. A comparison to realistic experimental conditions indicates that only one root remains practically observable in present devices such as NSTX, the slowly rotating, near-marginal stability S root that is identified as the resistive wall mode. In future devices with lower rotation and lower collisionality, the two rotating roots may become more important, but our analysis indicates that these roots are still likely to remain stable.

ACKNOWLEDGMENTS

The authors would like to acknowledge R. E. Bell and B. P. LeBlanc for diagnostic contributions to the experimental profiles in Fig. 1. Supported by the U.S. Department of Energy under Contract Nos. DE-FG02-99ER54524, DE-AC02-09CH11466, and DE-FG02-93ER54215.

APPENDIX A: ITERATION AND THE PERTURBATIVE APPROACH

There are two general approaches for the calculation of RWM stability, a calculation of a self-consistent set of equations for ξ and ω used, for example, by the MARS-K code, and the perturbative method, used in the simple model here and by the MISK code, of calculating the δW terms separately from a fixed ξ and then using Eq. (1) for ω. It is possible that in the self-consistent approach, ω is self-regulated in the sense that large $\hat{\omega}_r$, for example, could change ξ in such a way that ω is modified from the solutions given here.[9] It is worthwhile, however, to now consider which root the perturbative approach, used in the simple model presented here, finds more generally in the full MISK calculation.

An iterative method was developed for the perturbative MISK code to include the non-linear effect of $(\hat{\omega}_r, \hat{\gamma})$ appearing in Eq. (3) (Ref. 17). Near-zero values of $(\hat{\omega}_r, \hat{\gamma})$ are used in the first step, δW_K is calculated, and then $(\hat{\omega}_r, \hat{\gamma})$ are obtained from Eq. (1). These values are fed back as input into the δW_K calculation and iterated in this way until convergence is achieved. This method works well for the refinement of the single root found with MISK and has been shown to make little difference to the outcome as long as τ_w is not too low.[17]

Through experience, however, we have found that this iterative method never leads to convergence on a second or third root. We believe that this is because the single root found by MISK is what is known as an attracting fixed point, while the other two are repelling fixed points. If Eq. (1) is written $\hat{\omega} = f(\hat{\omega})$, then

$$f'(\hat{\omega}) = -\frac{\partial C}{\partial \hat{\omega}} \frac{\hat{\omega} + i}{\hat{\gamma}_f^{-1} + C}, \tag{A1}$$

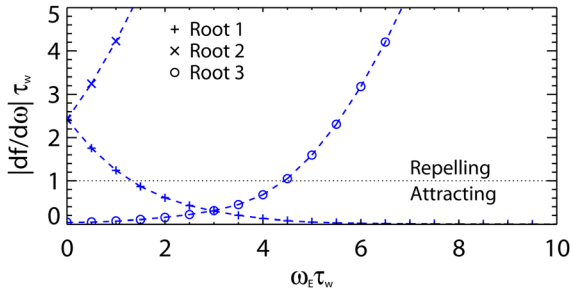

FIG. 7. (Color online) $|f'(\hat{\omega})|$ vs. $\hat{\omega}_E$ for the three analytical roots from Fig. 4.

and when $|f'(\hat{\omega})| < 1$, $\hat{\omega}$ is an attracting fixed point and iteration with values around that $\hat{\omega}$ will lead to convergence upon it (and the opposite for repelling fixed points).[28] Though a mathematical proof of this for the RWM roots for the full energy-dependent MISK calculation would be difficult, given the complexity, the observed behavior is consistent with this description.

We believe that the root which has $|\hat{\omega}_r|$ closest to zero (the S root, which is the most physically realistic representative of the true resistive wall mode seen in experiments), is always a fixed point root in our simple iterative scheme. Therefore the single root that is found by the full MISK calculation for experimental equilibria is the desired RWM root.

For the collisionless analytical case, we can calculate $|f'(\hat{\omega})|$, from Eqs. (5) and (A1), and plot it vs. $\hat{\omega}_E$ for the three analytical roots from Fig. 4. This is shown in Fig. 7 and it confirms that only the roots with low $|\omega_r|$ (root 1 at $\hat{\omega}_E > 1.4$ and root 3 at $\hat{\omega}_E > 4.4$) are attracting.

More sophisticated root finding techniques could be employed in the future to find the other two roots with MISK, including the use of a relaxation parameter to convert the rotating repelling fixed point roots to attracting, and the use of better initial guesses for $\hat{\omega}_r$ and $\hat{\gamma}$ for those roots.

APPENDIX B: ANALYTICAL SOLUTION

A convenient solution for Eq. (5) with $\hat{\nu} = 0$ can be found in the form of the solution to the cubic relation

$$z^3 + b_1 z^2 + b_2 z + b_3 = 0, \tag{B1}$$

with

$$z = -i(\hat{\omega} - \hat{\omega}_E), \tag{B2}$$

$$b_1 = \frac{2c - 1}{2c - \hat{\gamma}_f^{-1}} - i\hat{\omega}_E, \tag{B3}$$

$$b_2 = \frac{2c\hat{\omega}_{*N}\hat{\omega}_D + \hat{\gamma}_f^{-1}\hat{\omega}_D^2}{2c - \hat{\gamma}_f^{-1}}, \tag{B4}$$

$$b_3 = \frac{2c\hat{\omega}_{*N}\hat{\omega}_D - \hat{\omega}_D^2 - i\hat{\omega}_E\left(2c\hat{\omega}_{*N}\hat{\omega}_D + \hat{\gamma}_f^{-1}\hat{\omega}_D^2\right)}{2c - \hat{\gamma}_f^{-1}}. \tag{B5}$$

When $\omega_E = 0$, the coefficients of the cubic equation are real and then the fact that the discriminant

$$\Delta = 18b_1b_2b_3 - 4b_1^3b_3 + b_1^2b_2^2 - 4b_2^3 - 27b_3^2 \qquad \text{(B6)}$$

is less than zero means that one root of z is real and the other two are complex conjugates. This translates into one root having $\hat{\omega}_r = 0$ at $\hat{\omega}_E = 0$, while the other two have the same $\hat{\gamma}_0$ and $\hat{\omega}_r = \pm\hat{\omega}_0$, as was noted in Subsection IV A and Fig. 4.

[1]M. S. Chu and M. Okabayashi, Plasma Phys. Controlled Fusion **52**, 123001 (2010).
[2]S. A. Sabbagh, R. E. Bell, J. E. Menard, D. A. Gates, A. C. Sontag, J. M. Bialek, B. P. LeBlanc, F. M. Levinton, K. Tritz, and H. Yuh, Phys. Rev. Lett. **97**, 045004 (2006).
[3]R. Betti and J. P. Freidberg, Phys. Rev. Lett. **74**, 2949 (1995).
[4]R. Fitzpatrick and A. Y. Aydemir, Nucl. Fusion **36**, 11 (1996).
[5]R. Fitzpatrick, Phys. Plasmas **9**, 3459 (2002).
[6]A. Bondeson and M. S. Chu, Phys. Plasmas **3**, 3013 (1996).
[7]B. Hu and R. Betti, Phys. Rev. Lett. **93**, 105002 (2004).
[8]Y. Liu, M. S. Chu, I. T. Chapman, and T. C. Hender, Phys. Plasmas **15**, 112503 (2008).
[9]Y. Liu, I. T. Chapman, M. S. Chu, H. Reimerdes, F. Villone, R. Albanese, G. Ambrosino, A. M. Garofalo, C. G. Gimblett, R. J. Hastie, T. C. Hender, G. L. Jackson, R. J. La Haye, M. Okabayashi, A. Pironti, A. Portone, G. Rubinacci, and E. J. Strait, Phys. Plasmas **16**, 056113 (2009).
[10]Y. Liu, Nucl. Fusion **50**, 095008 (2010).
[11]A. H. Boozer, Phys. Plasmas **10**, 1458 (2003).
[12]B. Hu, R. Betti, and J. Manickam, Phys. Plasmas **12**, 057301 (2005).
[13]M. Ono, S. M. Kaye, Y. K. Peng, G. Barnes, W. Blanchard, M. D. Carter, J. Chrzanowski, L. Dudek, R. Ewig, D. Gates, R. E. Hatcher, T. Jarboe, S. C. Jardin, D. Johnson, R. Kaita, M. Kalish, C. E. Kessel, H. W. Kugel, R. Maingi, R. Majeski, J. Manickam, B. McCormack, J. Menard, D. Mueller, B. A. Nelson, B. E. Nelson, C. Neumeyer, G. Oliaro, F. Paoletti, R. Parsells, E. Perry, N. Pomphrey, S. Ramakrishnan, R. Raman, G. Rewoldt, J. Robinson, A. L. Roquemore, P. Ryan, S. Sabbagh, D. Swain, E. J. Synakowski, M. Viola, M. Williams, and J. R. Wilson, Nucl. Fusion **40**, 557 (2000).
[14]I. T. Chapman, C. G. Gimblett, M. P. Gryaznevich, T. C. Hender, D. F. Howell, Y. Q. Liu, and S. D. Pinches, Plasma Phys. Controlled Fusion **51**, 055015 (2009).
[15]M. Okabayashi, I. N. Bogatu, M. S. Chance, M. S. Chu, A. M. Garofalo, Y. In, G. L. Jackson, R. J. La Haye, M. J. Lanctot, J. Manickam, L. Marrelli, P. Martin, G. A. Navratil, H. Reimerdes, E. J. Strait, H. Takahashi, A. S. Welander, T. Bolzonella, R. V. Budny, J. S. Kim, R. Hatcher, Y. Q. Liu, and T. C. Luce, Nucl. Fusion **49**, 125003 (2009).
[16]G. Matsunaga, K. Shinohara, N. Aiba, Y. Sakamoto, A. Isayama, N. Asakura, T. Suzuki, M. Takechi, N. Oyama, and H. Urano, Nucl. Fusion **50**, 084003 (2010).
[17]J. W. Berkery, S. A. Sabbagh, H. Reimerdes, R. Betti, B. Hu, R. E. Bell, S. P. Gerhardt, J. Manickam, and M. Podesta, Phys. Plasmas **17**, 082504 (2010).
[18]G. Z. Hao, Y. Q. Liu, A. K. Wang, H. B. Jiang, G. Lu, H. D. He, and X. M. Qiu, Phys. Plasmas **18**, 032513 (2011).
[19]J. W. Berkery, S. A. Sabbagh, R. Betti, R. E. Bell, S. P. Gerhardt, B. P. LeBlanc, and H. Yuh, Phys. Rev. Lett. **106**, 075004 (2011).
[20]H. Reimerdes, A. M. Garafalo, M. Okabayashi, E. J. Strait, R. Betti, M. S. Chu, B. Hu, Y. In, G. L. Jackson, R. La Haye, M. Lanctot, Y. Liu, G. Navratil, W. Solomon, H. Takahashi, R. Groebner, and the DIII-D team, Plasma Phys. Controlled Fusion **49**, B349 (2007).
[21]B. Hu, R. Betti, and J. Manickam, Phys. Plasmas **13**, 112505 (2006).
[22]J. W. Berkery, S. A. Sabbagh, R. Betti, B. Hu, R. E. Bell, S. P. Gerhardt, J. Manickam, and K. Tritz, Phys. Rev. Lett. **104**, 035003 (2010).
[23]S. A. Sabbagh, J. W. Berkery, R. E. Bell, J. M. Bialek, S. P. Gerhardt, J. E. Menard, R. Betti, D. A. Gates, B. Hu, O. N. Katsuro-Hopkins, B. P. LeBlanc, F. M. Levinton, J. Manickam, K. Tritz, and H. Yuh, Nucl. Fusion **50**, 025020 (2010).
[24]W. Zhu, S. A. Sabbagh, R. E. Bell, M. G. Bell, B. P. LeBlanc, S. M. Kaye, F. M. Levinton, J. E. Menard, K. C. Shaing, A. C. Sontag, and H. Yuh, Phys. Rev. Lett. **96**, 225002 (2006).
[25]H. Reimerdes, J. W. Berkery, M. J. Lanctot, A. M. Garofalo, J. M. Hanson, Y. In, M. Okabayashi, S. A. Sabbagh, and E. J. Strait, Phys. Rev. Lett. **106**, 215002 (2011).
[26]K. C. Shaing, Phys. Plasmas **11**, 5525 (2004).
[27]A. C. Sontag, S. A. Sabbagh, W. Zhu, J. E. Menard, R. E. Bell, J. M. Bialek, M. G. Bell, D. A. Gates, A. H. Glasser, B. P. LeBlanc, K. C. Shaing, D. Stutman, and K. Tritz, Nucl. Fusion **47**, 1005 (2007).
[28]J. Milnor, *Dynamics in One Complex Variable* (Princeton University Press, Princeton, NJ, 2006).